Article

Computational modeling of biomechanics and biorheology of heated red blood cells

Zixiang Leonardo Liu,[1,*] He Li,[2,*] Yuhao Qiang,[4] Pierre Buffet,[3] Ming Dao,[4] and George Em Karniadakis[1,2,*]

[1]Division of Applied Mathematics, Brown University, Providence, Rhode Island; [2]School of Engineering, Brown University, Providence, Rhode Island; [3]Université Paris Descartes, Institut National de la Transfusion Sanguine, Paris, France; and [4]Department of Materials Science and Engineering, Massachusetts Institute of Technology, Cambridge, Massachusetts

ABSTRACT Because of their compromised deformability, heat denatured erythrocytes have been used as labeled probes to visualize spleen tissue or to assess the ability of the spleen to retain stiff red blood cells (RBCs) for over three decades, e.g., see Looareesuwan et al. *N. Engl. J. Med.* (1987). Despite their good accessibility, it is still an open question how heated RBCs compare to certain diseased RBCs in terms of their biomechanical and biorheological responses, which may undermine their effective usage and even lead to misleading experimental observations. To help answering this question, we perform a systematic computational study of the hemorheological properties of heated RBCs with several physiologically relevant static and hemodynamic settings, including optical-tweezers test, relaxation of prestretched RBCs, RBC traversal through a capillary-like channel and a spleen-like slit, and a viscometric rheology test. We show that our in silico RBC models agree well with existing experiments. Moreover, under static tests, heated RBCs exhibit deformability deterioration comparable to certain disease-impaired RBCs such as those in malaria. For RBC traversal under confinement (through microchannel or slit), heated RBCs show prolonged transit time or retention depending on the level of confinement and heating procedure, suggesting that carefully heat-treated RBCs may be useful for studying splenic- or vaso-occlusion in vascular pathologies. For the rheology test, we expand the existing bulk viscosity data of heated RBCs to a wider range of shear rates ($1–1000$ s^{-1}) to represent most pathophysiological conditions in macro- or microcirculation. Although heated RBC suspension shows elevated viscosity comparable to certain diseased RBC suspensions under relatively high shear rates ($100–1000$ s^{-1}), they underestimate the elevated viscosity (e.g., in sickle cell anemia) at low shear rates (<10 s^{-1}). Our work provides mechanistic rationale for selective usage of heated RBC as a potentially useful model for studying the abnormal traversal dynamics and hemorheology in certain blood disorders.

SIGNIFICANCE Heat denatured erythrocytes because of their compromised deformability have been used as labeled probes to visualize spleen tissue or to assess the ability of the spleen to retain stiff red blood cells (RBCs). Despite their good accessibility, how heated RBCs compare to certain diseased RBCs in terms of their biomechanical and biorheological responses is still an open question. Here, we perform a systematic computational study of the single cell mechanics and hemorheological properties of heated RBCs, and our results demonstrate the capability of heated RBC as a potentially useful model for studying the abnormal traversal dynamics and hemorheology in certain blood disorders.

INTRODUCTION

While traveling in the blood circulation, the red blood cell (RBC) has to repeatedly traverses through capillaries or microvascular beds and undergoes drastic deformation to

successfully transport oxygen and nutrients throughout the body, all attributed to its amazing deformability (1–3). Hereditary blood disorders such as spherocytosis, elliptocytosis, ovalocytosis, sickle cell anemia, or acquired hemotologic diseases such as type II diabetic mellitus and malaria all exhibit certain loss of RBC deformability (2,4–9), leading to severe and even life-threatening vascular complications such as vaso-occlusion and spleen sequestration (6,10,11). Understanding how the deterioration in RBC deformability alters the normal hemodynamics in vascular systems at both the single cell level as well as bulk suspension level may help in identifying

novel intervention strategies for these hemotologic disorders.

Heat treatment of RBCs has been a popular procedure to artificially increase the rigidity of RBC in a irreversible manner (12,13). Owing to its good accessibility and significantly altered cell deformability, heated RBCs have been used as a RBC model or biomarkers for accessing splenic or hepatic functions in hematologic disorders such as malaria and sickle cell disease (1,4–20). Compared with normal healthy RBCs, heated RBCs show enhanced membrane stiffness (13) and up to 10% increase of effective volume (reflected in apparent hematocrit), depending on the time duration of heating (21). At the molecular level, heat stresses were found to induce the dissociation of the membrane spectrin dimer into monomers (22), possibly explaining the stiffening of the RBC membrane. Despite certain structural understanding and good accessibility of heated RBCs, it remains quantitatively elusive exactly how heated RBCs compare to diseased RBCs in terms of the biomechanical and biorheological responses. Recent experimental evidence using microfluidic filtration systems on stiffened RBCs because of sickle cell disease (23,24) suggests that heated RBCs with stiffened membrane shear modulus may show similar clogging behavior compared to diseased RBCs such as those in sickle cell disease patients (see Fig. 1 A). Existing experimental measurements of the cell membrane mechanical properties (5,13,25) also point to comparable stiffening of the cell membrane between heated cells and diseased cells (e.g., Fig. 1 B). Such experimental evidence suggests the need for a more comprehensive understanding of the biomechanics and biorheology of heated RBCs under specific microfluidic settings, which may provide better guidance for their effective usage as controls or surrogates for studying red cell diseases.

The last 10 years have witnessed considerable development of multiscale computational models that allow in silico investigation of RBC disorders from single cell mechanics (26–32) to cellular blood flow dynamics (33–41);

e.g., see recent reviews (42–45). To access the potential feasibility of utilizing heated RBCs as surrogates or controls for studying blood disorders, we leverage multiscale computational blood flow simulations to systematically evaluate the cell mechanics, traversal dynamics, and hemorheology of heated RBCs under various physiologically relevant settings. We show that our predictions for heated RBCs agree well with existing experiments. Moreover, we find that heated RBCs can produce representative mechanical or rheological characteristics in certain blood disorders under specific hemodynamic conditions. Our results can serve as a benchmark for the hemorheological properties of heated RBCs, and they can also provide possible guidance for selective usage of heated RBCs as abnormal blood surrogates under specific physiologically relevant settings.

MATERIALS AND METHODS

Dissipative particle dynamics model for the fluid phase

The suspended blood plasma are modeled using the dissipative particle dynamics (DPD) (46). The DPD particles interact with each other through soft pairwise forces, including conservative, dissipative, and random forces. The dissipative and random forces are determined through the fluctuation-dissipation theorem, together forming a thermostat for the suspension systems. The viscosity of the system is an outcome of the combination of these three forces (47) and needs to be measured a priori for proper mapping between the physical unit and DPD unit (26,33). Following a previous study (33), a single solvent (both plasma and cytoplasm) viscosity of 1.2 cP is used for current simulations, which substantially reduces the computational cost and allows us to simulate a physiological hematocrit (45%) of RBC suspensions over a wide range of shear rates. The temperature is set to room temperature of 310 K. The formulation of potentials applied in the DPD model is introduced in Supporting materials and methods, and model parameters are listed in Table S1.

Coarse-grained RBC membrane model

The RBC model used in this work is based on the coarse-grained membrane model developed in Fedosov et al. (26). The RBC membrane
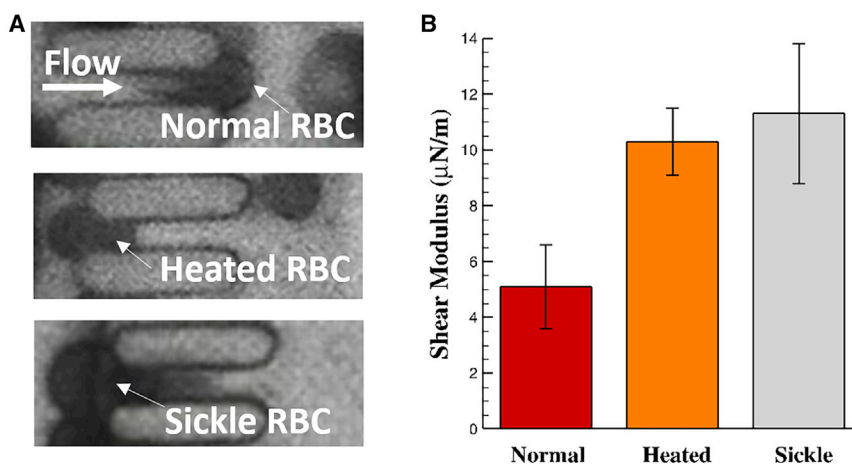
FIGURE 1 Heated RBCs can clog the microfluidic filtration system similarly compared with sickle RBCs under normoxia. (A) Both heated RBCs and sickle RBCs get retained by the narrow slit-shaped microgate, whereas normal RBCs pass through. The experimental setup is described in our previously published work (23), except the microgate opening has changed to 2 μm wide and 20 μm long. Flow is from left to right. (B) Existing literature suggests that heated RBCs (13) and sickle RBCs under normoxia (25) show a similar elevation of shear modulus compared with normal RBCs (5). The error bars are directly adopted from the literature (5,3,25). To see this figure in color, go online.

visco-elasticity is mainly determined by the membrane cytoskeleton, namely the spectrin network, whereas bending is controlled by the lipid bilayer. In this model, the RBC membrane is approximated as a one-component collection of membrane vertices connected by hyperelastic springs. The rigorous coarse-graining procedure allows for the flexibility of using a different number of vertices to represent the RBC membrane while preserving the accurate cell membrane mechanical and rheological properties (48). Specifically, the model incorporates the bending energy, in-plane shear energy, membrane viscosity, and area and volume constraints. To be coupled with the fluid phase, the vertices on the RBC membrane are also treated as the DPD particles. Therefore, each vertice also experiences DPD forces from the internal and external fluid particles of the cell in addition to the membrane model forces. The formulation of potentials applied in the RBC model is introduced in Supporting materials and methods, and model parameters are listed in Tables S2 and S3.

Problem setup

Previously, Nash and Meiselman (13) demonstrated that RBCs treated with heat at 48 ± 0.5°C for ~9 min could lead to irreversible stiffening of the RBC membrane with minor change to the RBC shape and morphorlogy; rheologic tests of the heated RBCs reported a ~2.4-fold increase in membrane shear modulus and a ~1.3-fold increase in membrane viscosity. In another set of experiments by Ham et al. (21), the heat treatment of RBCs was prolonged to up to 60 min. They observed that in addition to the membrane stiffening, a change of cell morphology also occurred, causing a roughly 10% increase in apparent hematocrit. To reflect these experimental observations, we propose two types of heated RBC models. The short-duration heated RBC (SH-RBC) model considers only the heat-altered membrane properties. In addition to the membrane alteration, the long-duration heated RBC (LH-RBC) model further assumes a 10% increase in cell volume. The RBC mechanical properties for normal RBC (N-RBC) and heated RBCs are tabulated in Table 1.

Simulation results

In the following sections, we systematically examine the static, dynamic, and rheological responses of the two models for heated RBCs in comparison with normal RBCs and various types of impaired RBCs in vascular diseases. We first focus on interrogating the single cell static responses. Then, our focus is shifted to understanding the traversal dynamics of normal and heated RBCs flowing through capillary-like microchannels and splenic slits. Last, we examine the macroscopic viscosity of RBC suspensions (or blood) over a wide range of shear rate changing from 1 to 1000 s^{-1} to cover the majority of hemorheological conditions in blood circulation (3,50).

Optical-tweezers test

Optical-tweezers stretching experiments are standard tests for probing the single cell elastic responses (51). Here, we perform stretching tests of

TABLE 1   Mechanical properties of normal RBCs versus heated RBCs

Cell Properties	N-RBC	SH-RBC	LH-RBC
Shear modulus, G (μN/m)	4.3 (5)	10.3 (13)	10.3 (5)
Membrane viscosity, η (*Pa* s)	0.128 (27)	0.166 (13)	0.166 (13)
S/V (μm^{-1})	1.43 (49)	1.43 (49)	1.30 (21)

The mechanical properties for N-RBC are within the range of previous measurements (5,27,49). The membrane properties for SH-RBC and LH-RBC are based on the experimental measurements by Nash and Meiselman (13) and Ham et al. (21).

model N-RBC and heated RBC (SH-RBC and LH-RBC) and compare our results with existing measurements of RBC deformation under various pathophysiological conditions (5,8). Following previous work (26), the stretching force changes from 0 to 200 pN. The cell deformation is monitored by the change of diameters of the cell along axial (D_A) and transverse (D_T) directions with respect to the direction of the stretching force, as depicted in Fig. 2 A. During the test, RBC elongates in the axial direction while contracting in the transverse direction. As shown in Fig. 2 A, SH-RBC shows less elongation compared with N-RBC under a stretching force of 100 pN, confirming the stiffening of the heated RBC membrane.

Fig. 1 B further summarizes the change of D_A and D_T associated with different levels of the loading force. Our predicted RBC deformation for normal RBCs compares quantitatively well with the experimental results reported in Suresh et al. (5), showing the validity of our model. Compared with N-RBC, both SH-RBC and LH-RBC show compromised deformation as a result of the elevated elastic shear modulus (13). The deformation of SH-RBC and LH-RBC is almost identical, suggesting the ~10% increase of volume in LH-RBC is not significant to cause an extra stretching response. Notably, RBC parasitized by *Plasmodium falciparum* at ring stage (5) in malaria patients and patients with type II diabetes mellitus (8) show similar stretching response compared with heated RBCs, especially in the axial deformation (D_A). These results suggest that the membrane elasticity of heated RBCs may be similar to those in certain diseased RBCs, but such conjecture remains to be confirmed through more definitive experimental tests.

Cell relaxation in quiescent flows

The timescale to recover the equilibrium morphology of an RBC after releasing from a stretching force can be used to quantify the cell membrane viscosity through calculating a membrane time constant (52). The quantification process typically requires introducing a time-dependent relaxation index, $R(t)$, defined as:

$$R(t) = \frac{(\lambda - \lambda_\infty)(\lambda_0 + \lambda_\infty)}{(\lambda + \lambda_\infty)(\lambda_0 - \lambda_\infty)}, \tag{1}$$

to be fitted with an exponential functional form, $\exp\left[-\left(\frac{t}{t_c}\right)^\sigma\right]$, where the ratios $\lambda(t) = D_A/D_T$, $\lambda_0 = D_A^0/D_T^0$, and $\lambda_\infty = D_A^\infty/D_T^\infty$ are the ratios at time zero and in the long-time asymptotic state, respectively. The exponent σ is set to 0.7 following previous work (53). The time constant, t_c, can be extracted from the curve fitting procedure (52).

Fig. 3 A demonstrates the temporal change of the cell morphology, in which heated RBC (taking SH-RBC as an example) restore to their equilibrium shape in ~0.7 s in contrast to the ~1.0 s required for the N-RBC. Fig. 3 B plots the time course of the preloaded stretching force, F, and the corresponding D_A and D_T, in which the difference between N-RBC and heated RBC is noticeable. Based on the data from Fig. 3 B, $R(t)$ is calculated and plotted against time in Fig. 3 C. We find that the N-RBC exhibits a time constant of t_c ~0.12 s, SH-RBC t_c ~0.075 s, and LH-RBC t_c ~0.06 s. As shown in Fig. 3 D, the measured t_c in our simulation for both the N-RBC and SH-RBC matches well with the experimental results in Nash et al. (13), hence validating our computational results. Interestingly, the LH-RBC constantly shows a relatively smaller t_c compared with SH-RBC, suggesting that the decreased surface/volume (S/V) ratio could also aid in the cell recovery process in addition to the increased cell membrane viscosity.

Single RBC traversal through a capillary-like microchannel

Although the static characteristics of single heated RBC have been measured previously in vitro (13), which we use to validate our RBC
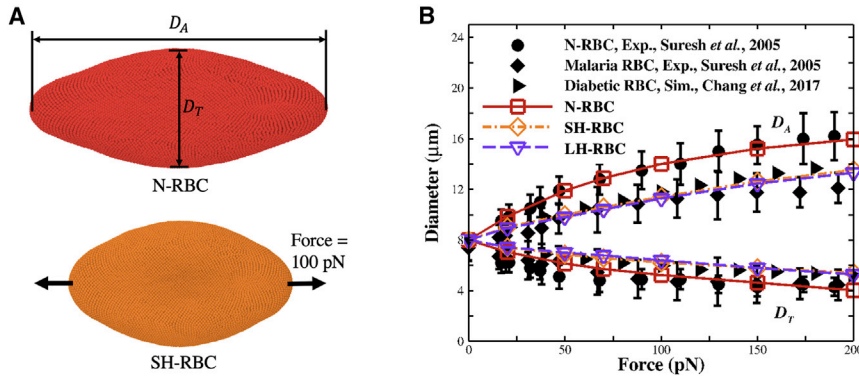
FIGURE 2 Static deformation responses of RBCs tested with optical tweezers. (A) Equilibrium deformation of N-RBCs versus SH-RBCs under an optical tweezer force of 100 pN. LH-RBC shows similar deformation compared with SH-RBC. (B) The change of RBC diameter along the axial (D_A) and transverse (D_T) directions subject to various optical-tweezer forces ranging from 0 to 200 pN. The experimental results from Suresh et al. (5) for N-RBC and malaria-infected RBC and simulation results from Chang et al. (8) are plotted for comparison. Lines with open symbols are from simulations. The error bars are adopted from the experiments (5). Black symbols are from previous experimental and simulation studies. To see this figure in color, go online.

model in previous sections, the dynamic response of heated RBCs under hydrodynamic stresses and confinement has largely remained unexplored. Yet this is paramount as RBCs are constantly subject to shear stresses and confinement in blood circulation, particularly in capillary beds (54). In this section, we model a single RBC flowing through a capillary-like microfluidic channel to quantify the traversal dynamics of normal and heated RBC in capillaries. The narrowed section of the microfluidic channel is 30 μm in length (x), 5 μm in width (y), and 2.7 μm in depth (z), as denoted in Fig. 4 B. Initially, the cell is placed at the inlet of the channel (on the left side of the constriction). A constant pressure drop across the channel is imposed to drive the flow, whereas periodic boundary conditions are applied to the inlet and outlet of the channel. This computational setup has been previously validated against our own experiment (55).

To delineate the traversal dynamics of the single RBC, we monitor the evolution of the cell morphology quantified by the maximal diameter in y direction (D_y) as well as the instantaneous cell velocity in x direction (V_x), as shown in Fig. 4 A. As indicated by the change of D_y, the cell undergoes a drastic narrowing to about the width of the channel while elongating along the streamwise direction. The slight lower value of D_y compared with the channel width indicates the formation of a lubrication layer between the cell and the channel wall. Three characteristic time points (i, ii, and iii) for the N-RBC case are further denoted in Fig. 4 A (top) to better understand the cell traversal dynamics. These times correspond to when the cell enters (i), squeezes through (ii), and exits (iii) the narrowed section of the channel, where the corresponding simulation snapshots are presented in Fig. 4 B. From time (i) to (ii), it is noteworthy that the cell undergoes a transition from deceleration to acceleration mode (Fig. 4 A). This can be explained
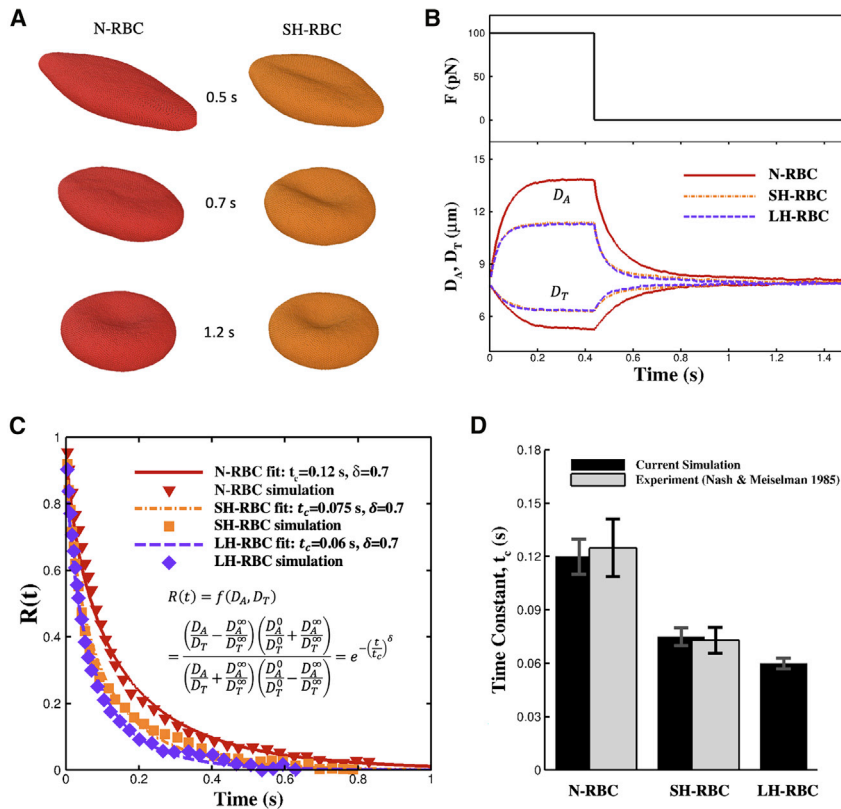
FIGURE 3 Relaxation of prestretched RBCs under no flow condition. (A) Snapshots of instantaneous RBC morphology under loading (0.5 s), during recovery with zero loading (0.7 s), and close to stress-free state (1.2 s). Compared with N-RBCs, heated RBCs show a more rapid relaxation response. SH-RBCs and LH-RBCs show similar relaxation responses. (B) Temporal change of RBC diameters (D_A and D_T) under a step change of stretching force, F, from 100 to 0 pN. (C) Evaluation of the RBC time constant based on the curve fitting procedure (52). The inset shows the fitting function for obtaining the time constant, t_c, based on the exponent, $\sigma = 0.7$ (8,53). (D) Time constant comparison between simulations and experiment (13). The error bar of t_c in simulations is obtained by varying the membrane viscosity within a range observed in a previous experiment (13). To see this figure in color, go online.
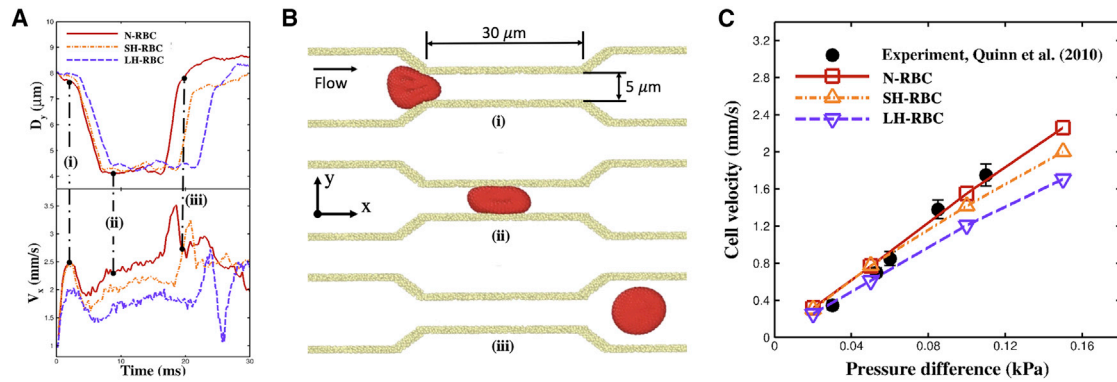
FIGURE 4 Traversal dynamics of a single RBC flowing through a capillary-like microfluidic channel designed in Quinn et al. (55). (A) Temporal change of cell diameter in the cross-stream (y) direction (*top*) and instantaneous velocity along the streamwise (x) direction (*bottom*) under a driving pressure difference of 0.15 kPa. (B) The simulation snapshots corresponding to the numbered time instances in (A) show a N-RBC entering (i), squeezing through (ii), and exiting (iii) the narrowed section of the microchannel. The channel dimension is denoted in the figure, where the depth of the channel is 2.7 μm (data not shown). Initially, all cells were located at the entrance of the channel (*left end* of the microfluidic channel). (C) Cell velocity (defined as the average of V_x over time) during stage (ii) plotted against different pressure differences. The experimental results with error bars from Quinn et al. (55) are plotted for comparison. To see this figure in color, go online.

by the RBC's adaptation to the constriction followed by an increase of its squeezing velocity as the cell squeezes through with no further blockage. As the cell leaves the narrowed section, the cell exhibits a greater acceleration because of the reduction of the cell-wall friction. Subsequently, the cell velocity abruptly drops (iii) as the cell recovers to its equilibrium state ($D_y \sim 8$ μm) and the corresponding hydrodynamic drag exerted on the cell increases. Compared with N-RBC, heated RBC shows a prolonged transit time as clearly indicated by the wider basin of the D_y curve and the lower level of V_x in Fig. 4 A. Quantitatively, the transit time for N-RBC, SH-RBC, and LH-RBC is 17.5, 20.0, and 25.0 ms, respectively, under the pressure difference of 0.15 kPa. The sudden drop of velocity at stage (iii) appears to be more drastic in LH-RBC compared with both SH-RBC and N-RBC, which suggests LH-RBC recovers shape and experiences an elevated hydrodynamic drag faster than the other two. This is in fact consistent with the shortest t_c of LH-RBC observed in the previous section.

Fig. 4 C depicts the average cell velocity with respect to various pressure difference levels. Our predicted cell velocity for N-RBC matches well with the experimental results by Quinn et al. (55), featuring a linear trend with respect to the pressure difference. While maintaining an almost linear scaling with pressure difference, cell velocities for SH-RBC and LH-RBC are reduced to various extents, particularly at the higher pressure differences, owing to the impaired cell deformability. Compared with N-RBC, the cell velocity is reduced by 15% for SH-RBC and 30% for LH-RBC under a pressure difference of 0.15 kPa.

Single RBC traversal through an interendothelial slit

The extreme deformation for RBCs during the blood circulation occurs when an RBC squeezes through the splenic sinus and interendothelial slits (IES) that typically feature an opening as small as $\sim$1.0 μm (56). To understand the traversal dynamics of heated RBC under such a severe confinement, we performed simulations to reconstruct the RBC passage process at a single IES under physiological conditions. Following previous works (7,32), we construct the IES geometry with a slit height of 1.2 μm, a width of 5.0 μm, and a depth of 2.5 μm. The initial position of the RBC is placed 9 μm upstream of the IES. The pressure drop across the slit to drive the flow is set to 6 Pa μm^{-1}, which is within the range of in vivo measurements (57). The simulation setup is depicted in Fig. 5 A.

The cell morphology for RBC just squeezing through (N-RBC and SH-RBC) or getting retained by (LH-RBC) the IES is depicted in Fig. 5 B,

where the times for each snapshot are denoted accordingly on the RBC traversal displacement plot shown in Fig. 5 C. The RBC traversal displacement is defined as the traveling distance of the RBC centroid in the streamwise direction. As shown in Fig. 5 C, all RBCs arrive at the IES in $\sim$50 ms. Subsequently, the cell starts to squeeze through the IES. The squeezing process is rather sluggish as the traversal displacement remains almost flat (Fig. 5 C), whereas the cell undergoes severe deformation. After lingering for more than 200 ms, the N-RBC completely squeezes through as the RBC traversal displacement starts to increase drastically. The SH-RBC owing to its stiffening of cell membrane requires twofold the normal passage time. In contrast, the LH-RBC is not able to squeeze through the IES after more than 1000 ms.

Comparing our predicted passage time with the counterparts measured in vivo by MacDonald et al. (56) (replotted in Fig. 5 C), we see that our N-RBC passage time aligns very well with the times that show the highest passage frequency, as shown in Fig. 5, C and D. The passage time for SH-RBC corresponds to a much lower passage frequency, whereas that for LH-RBC should fall in the scenario that the passage frequency is almost zero. We also tested one RBC model that has the N-RBC membrane property but with the S/V ratio of LH-RBC. We found that this RBC model also becomes retained (see Fig. 5 D). This suggests that the 10% increase of the RBC volume is the root cause for the change of traversal dynamics from passage to retention, whereas stiffening the membrane alone by 200–300% is not significant to cause a paradigm shift. Overall, our results confirm that RBC retention is more sensitive to the increase of RBC volume compared with membrane stiffening, consistent with the results shown in previous in vitro (7) and ex vivo (58,59) observations.

Rheology of RBC suspensions

The superior deformability of RBCs in blood suspension collectively determines the bulk rheology of the blood, giving rise to blood non-Newtonianity such as shear thinning and the Fåhræus–Lindqvist effect (60,61). Changes of RBC deformability at the cellular level often leads to abnormality in macroscopic rheology, which has been observed in a variety of hemotologic disorders (4,62–64). Previously, Nash and Melseiman (13) demonstrated elevated bulk viscosity of SH-RBC suspensions under physiologically high shear rates (100–1000 s^{-1}). Their results suggest that heated RBC suspension may be a good surrogate of diseased blood to study pathological mechanisms related to elevation in blood viscosity. To test this hypothesis, we compute the relative viscosity of heated RBC suspensions under shear

rates ranging from 1 to 1000 s^{-1}. This four orders of magnitude range covers most of the shear level present in micro- and macrocirculation (3,50). The hematocrit is set to 45% matching the physiological level. The shear cell considered in the current study (see the inset of Fig. 6) has a dimension of 50^3 μm^3 that was shown to be sufficiently large for accurate rheological characterization (33,65).

Fig. 6 summarizes the relative viscosity of RBC suspensions or blood under various pathophysiological conditions. In general, the blood shear thinning behavior is well captured by our model. Our predicted viscosities for the N-RBC show good agreement with the experimental results reported in Skalak et al. (49). Our predicted viscosity for SH-RBC shows ∼1.2 times elevation compared with normal over the entire shear rate range. At the physiologically high shear rates (100–1000 s^{-1}), our simulation compares well with the experimental results in Nash and Meiselman (13). The viscosity for LH-RBC is predicted to be further elevated by a ∼1.4-fold compared with normal values as a result of the increased effective hematocrit (21). Under physiologically high shear rates (>100 s^{-1}), the elevated viscosity of heated RBC suspensions seems to be representative of the rheological anomalies of various vascular diseases such as sickle cell anemia under oxygenation (63), diabetic blood (64), and malaria-infected blood (66). However, under lower shear rates (≪100 s^{-1}), the viscosity of heated RBC suspension could be significantly lower than those in pathologies, particularly in sickle cell anemia and diabetic mellitus. Our study suggests that hemorheolgical conditions such as shear rate may be an important factor to consider while accessing the feasibility of using heated RBCs as RBC models for blood abnormalities.

DISCUSSION

In this work, we systematically investigate the hemorheological properties of heated RBCs to evaluate the potential usage of heated RBCs as surrogates for studying hemotologic disorders. Our predictions for normal and heated RBCs show good agreement with existing in vitro and in vivo measurements in terms of the cell static and dynamic
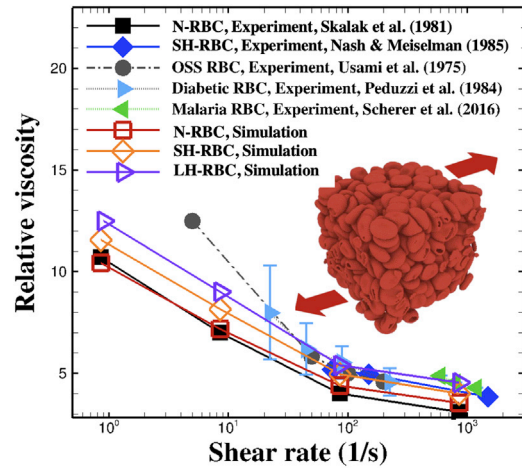
FIGURE 6 Blood relative viscosity for different hematologic disorders evaluated in viscometric flows under physiologically relevant shear rates ranging from 1 to 1000 s^{-1}. Experimental viscosity measurements for N-RBC suspension in ringer solution by Skalak et al. (49), SH-RBC suspension by Nash and Meiselman (13), oxygenated sickle blood by Usami et al. (63), blood from diabetic patients with retinopathy by Peduzzi et al. (64), and blood in malaria patients by Scherer et al. (66) are plotted to evaluate the usability of the heated RBC rheology. The blood viscosity computed in our simulations is normalized with the plasma viscosity, 1.2 cP, to obtain the relative viscosity. The viscosity measurements for malaria blood (66) and SH-RBC (13) were based on a hematocrit of ∼40% and were rescaled to 45% based on the previous calculations (33). Open symbols represent simulation results, whereas solid symbols represent experimental results. The error bars are adopted from the literature (64). To see this figure in color, go online.

and rheologic responses under a variety of physiologically relevant settings, demonstrating the validity and generality of our heated RBC model.
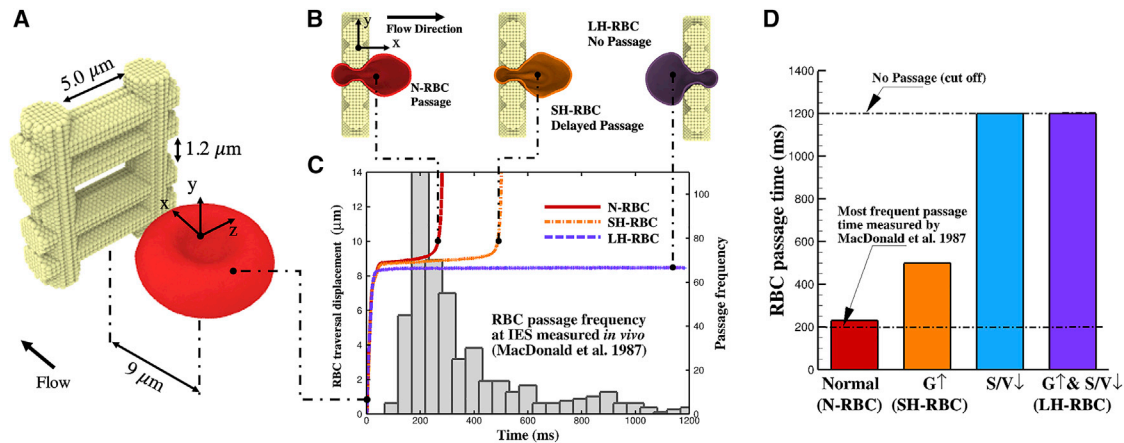
FIGURE 5 Traversal dynamics of RBC squeezing through a splenic slit. (A) The simulation setup. The IES has a slit height of 1.2 μm, a width of 5.0 μm, and slit depth of 2.5 μm. The RBC is initially positioned 9 μm upstream to the IES. A pressure gradient of 6 Pa μm^{-1} across the IES is applied to drive the flow along the x-direction. (B) Side views of a single RBC passing through the IES. The flow direction is as denoted. From left to right, N-RBC shows normal passage, SH-RBC shows delayed passage, and LH-RBC shows no passage (retention) at the IES, respectively. The snapshots were taken from the time points as denoted on the curves of (B). Half of the IES and RBC were hidden for better visualization. (C) RBC traversal displacement plotted against time. Note that the time origin for the RBC travesal displacement is shifted to when the RBC arrives at the IES. The passage frequency distribution for RBC through IES measured in vivo (56) is depicted for comparison. (D) RBC passage time comparison for RBCs with different mechanical properties because of heat treatment. The case with only S/V decrease (through increasing volume) is simulated to demonstrate its primary effect on cell passage over membrane stiffening (G increase). To see this figure in color, go online.

Our results further suggest the static stretching response of heated RBCs may be similar to those in malaria and type II diabetes mellitus. Although the mechanism that alters the cell membrane properties could be completely different pathologically or biologically (5,8), such results provide quantitative support for the usage of heated RBC as effective controls for studying an impaired RBC membrane for certain vascular diseases. However, further confirmatory studies through experiments need to be carried out to confirm this conjecture.

The significantly altered traversal dynamics in heated RBCs at the splenic IES is consistent with the previous usage of heated RBC as positive controls for studying splenic sequestration (59). Although the delayed passage due to membrane stiffening may eventually lead to the clogging of the IES, our simulation results suggest a more prominent contributor to the splenic occlusion with the heated RBC suspensions may be the RBCs with a slightly (∼10%) higher volume that are prevalent in LH-RBCs. This finding in the context of heated RBCs is in fact consistent with our previous observations in diseased RBCs such as those in malaria (7). Based on this knowledge, the ability of heated RBC suspensions for clogging the IES or small capillaries may be adjustable by controlling the fraction of LH-RBC through the heating time, which might be correlated to the severity of specific hemotologic disorders. Also, the marked distinct traversal responses of heated RBCs depending on the heating duration as confirmed by our simulations explains why strict respect of a specific heating protocol is essential for an appropriate interpretation of experimental results as well as for their repeatability and reproducibility. Note that previous ex vivo experiments by Safeukui et al. (58,59) showed that a 14–17% reduction in the S/V ratio of RBCs is needed to cause their retention. The slightly lower S/V ratio observed with our model may be related to subtle difference in pressure difference or slit dynamics (size or deformability) used in our model.

Previous experiments did not observe any significant change in RBC aggregation at low shear after heat treatment (67,68). These observations support our choice of not imposing extra cell-cell bridging effect for realistically modeling heated RBCs. Moreover, we predict that heated RBC suspensions without extra mechanisms for RBC agglutination tend to underpredict the severely elevated blood viscosity under low shear (<10 s^{-1}). Consequently, for studying vascular diseases involving relatively low shear conditions, e.g., those in saccular aneurysms (69) or deep venous thrombosis (70), in the context of elevated viscosity, using heated RBC suspension may undermine the viscous effect and hence underpredict the risk for rupture or vaso-occlusion. Nonetheless, this limitation of heated RBC may be overcome by adding plasma macromolecules such as fibrinogen to enhance the intercell bridging energy (71).

There are limitations to our computational study of the heated RBC hemorheology. We have neglected the heat-induced budding or hemolysis of RBCs observed in vitro (72), which, however, might be further investigated using the protein-level RBC models (29,73–75). The heterogeneity and polydispersity of heated RBCs under long-time (∼60 min) heating (21) are not considered in the current study, yet our study using a monodisperse RBC suspension seems to be sufficient in capturing the typical static, dynamic, and rheologic responses of heated RBCs. Overall, our in silico study confirms the potential usefulness of heated RBC as surrogates for certain blood disorders. Our work provides guidance and mechanistic rationale for the pinpointed usage of heated RBC as a potential diseased RBC model for studying the abnormal traversal dynamics and hemorheology in blood disorders.

SUPPORTING MATERIAL

Supporting material can be found online at https://doi.org/10.1016/j.bpj.2021.09.038.

AUTHOR CONTRIBUTIONS

H.L. and G.E.K. designed research. Z.L.L. and H.L. performed research. All authors analyzed the data and wrote the article.

ACKNOWLEDGMENTS

REFERENCES

1. Looareesuwan, S., M. Ho, …, D. J. Wyler. 1987. Dynamic alteration in splenic function during acute falciparum malaria. *N. Engl. J. Med.* 317:675–679.

2. Mohandas, N., and E. Evans. 1994. Mechanical properties of the red cell membrane in relation to molecular structure and genetic defects. *Annu. Rev. Biophys. Biomol. Struct.* 23:787–818.

3. Secomb, T. W. 1995. Mechanics of blood flow in the microcirculation. *Symp. Soc. Exp. Biol.* 49:305–321.

4. Chien, S., S. Usami, and J. F. Bertles. 1970. Abnormal rheology of oxygenated blood in sickle cell anemia. *J. Clin. Invest.* 49:623–634.

5. Suresh, S., J. Spatz, …, T. Seufferlein. 2005. Connections between single-cell biomechanics and human disease states: gastrointestinal cancer and malaria. *Acta Biomater.* 1:15–30.

6. Safeukui, I., J.-M. Correas, …, P. A. Buffet. 2008. Retention of Plasmodium falciparum ring-infected erythrocytes in the slow, open microcirculation of the human spleen. *Blood.* 112:2520–2528.

7. Pivkin, I. V., Z. Peng, …, S. Suresh. 2016. Biomechanics of red blood cells in human spleen and consequences for physiology and disease. *Proc. Natl. Acad. Sci. USA.* 113:7804–7809.

8. Chang, H.-Y., X. Li, and G. E. Karniadakis. 2017. Modeling of biomechanics and biorheology of red blood cells in type 2 diabetes mellitus. *Biophys. J.* 113:481–490.

9. Lei, H., and G. E. Karniadakis. 2012. Quantifying the rheological and hemodynamic characteristics of sickle cell anemia. *Biophys. J.* 102:185–194.

10. Buffet, P. A., I. Safeukui, …, P. H. David. 2009. Retention of erythrocytes in the spleen: a double-edged process in human malaria. *Curr. Opin. Hematol.* 16:157–164.

11. Lei, H., and G. E. Karniadakis. 2013. Probing vasoocclusion phenomena in sickle cell anemia via mesoscopic simulations. *Proc. Natl. Acad. Sci. USA.* 110:11326–11330.

12. Rakow, A. L., and R. M. Hochmuth. 1975. Effect of heat treatment on the elasticity of human erythrocyte membrane. *Biophys. J.* 15:1095–1100.

13. Nash, G. B., and H. J. Meiselman. 1985. Alteration of red cell membrane viscoelasticity by heat treatment: effect on cell deformability and suspension viscosity. *Biorheology.* 22:73–84.

14. Atkins, H. L., A. G. Goldman, …, S. C. Srivastava. 1980. Splenic sequestration of 99mTc labeled, heat treated red blood cells. *Radiology.* 136:501–503.

15. Lecklin, T., S. Egginton, and G. B. Nash. 1996. Effect of temperature on the resistance of individual red blood cells to flow through capillary-sized apertures. *Pflugers Arch.* 432:753–759.

16. Snowdon, G. M. 1998. A safe, simple method for preparing heat-damaged red cells for diagnosing splenic infarct or trauma. *J. Nucl. Med. Technol.* 26:204–205.

17. Buffet, P. A., G. Milon, …, P. H. David. 2006. Ex vivo perfusion of human spleens maintains clearing and processing functions. *Blood.* 107:3745–3752.

18. Jolepalem, P., and H. R. Balon. 2015. Application of heat-damaged Tc-99m RBCs in a patient with suspected hepatic metastasis. *Radiol. Case Rep.* 8:787.

19. Xu, T., M. A. Lizarralde-Iragorri, …, B. Le Pioufle. 2020. Characterization of red blood cell microcirculatory parameters using a bio-impedance microfluidic device. *Sci. Rep.* 10:9869.

20. Sammartano, A., M. Scarlattei, …, L. Ruffini. 2019. Validation of in vitro labeling method for human use of heat-damage red blood cells to detect splenic tissue and hemocateretic function. *Acta Biomed.* 90:275–280.

21. Ham, T. H., S. C. Shen, …, W. Castle. 1948. Studies on the destruction of red blood cells; thermal injury; action of heat in causing increased spheroidicity, osmotic and mechanical fragilities and hemolysis of erythrocytes; observations on the mechanisms of destruction of such erythrocytes in dogs and in a patient with a fatal thermal burn. *Blood.* 3:373–403.

22. Yoshino, H., and O. Minari. 1987. Heat-induced dissociation of human erythrocyte spectrin dimer into monomers. *Biochim. Biophys. Acta.* 905:100–108.

23. Du, E., M. Diez-Silva, …, S. Suresh. 2015. Kinetics of sickle cell biorheology and implications for painful vasoocclusive crisis. *Proc. Natl. Acad. Sci. USA.* 112:1422–1427.

24. Li, X., E. Du, …, G. E. Karniadakis. 2017. Patient-specific modeling of individual sickle cell behavior under transient hypoxia. *PLoS Comput. Biol.* 13:e1005426.

25. Nash, G. B., C. S. Johnson, and H. J. Meiselman. 1984. Mechanical properties of oxygenated red blood cells in sickle cell (HbSS) disease. *Blood.* 63:73–82.

26. Fedosov, D. A., B. Caswell, and G. E. Karniadakis. 2010. A multiscale red blood cell model with accurate mechanics, rheology, and dynamics. *Biophys. J.* 98:2215–2225.

27. Peng, Z., X. Li, …, S. Suresh. 2013. Lipid bilayer and cytoskeletal interactions in a red blood cell. *Proc. Natl. Acad. Sci. USA.* 110:13356–13361.

28. Li, X., Z. Peng, …, G. E. Karniadakis. 2014. Probing red blood cell mechanics, rheology and dynamics with a two-component multiscale model. *Philos. Trans.- Royal Soc., Math. Phys. Eng. Sci.* 372:20130389.

29. Tang, Y.-H., L. Lu, …, G. E. Karniadakis. 2017. OpenRBC: a fast simulator of red blood cells at protein resolution. *Biophys. J.* 112:2030–2037.

30. Zhu, Q., S. Salehyar, …, R. J. Asaro. 2017. Prospects for human erythrocyte skeleton-bilayer dissociation during splenic flow. *Biophys. J.* 113:900–912.

31. Salehyar, S., and Q. Zhu. 2017. Effects of stiffness and volume on the transit time of an erythrocyte through a slit. *Biomech. Model. Mechanobiol.* 16:921–931.

32. Li, H., L. Lu, …, S. Suresh. 2018. Mechanics of diseased red blood cells in human spleen and consequences for hereditary blood disorders. *Proc. Natl. Acad. Sci. USA.* 115:9574–9579.

33. Fedosov, D. A., W. Pan, …, G. E. Karniadakis. 2011. Predicting human blood viscosity in silico. *Proc. Natl. Acad. Sci. USA.* 108:11772–11777.

34. Liu, Z., Y. Zhu, …, C. K. Aidun. 2018. Nanoparticle transport in cellular blood flow. *Comput. Fluids.* 172:609–620.

35. Balogh, P., and P. Bagchi. 2018. Analysis of red blood cell partitioning at bifurcations in simulated microvascular networks. *Phys. Fluids.* 30:051902.

36. Liu, Z., J. R. Clausen, …, C. K. Aidun. 2019. A unified analysis of nano-to-microscale particle dispersion in tubular blood flow. *Phys. Fluids.* 31:081903.

37. Liu, Z., Y. Zhu, …, C. K. Aidun. 2019. Multiscale method based on coupled lattice-Boltzmann and Langevin-dynamics for direct simulation of nanoscale particle/polymer suspensions in complex flows. *Int. J. Numer. Methods Fluids.* 91:228–246.

38. Zhao, H., and E. S. G. Shaqfeh. 2020. Shear-induced platelet margination in a microchannel. *Phys. Rev. E.* 83:061924.

39. Deng, Y., D. P. Papageorgiou, …, G. E. Karniadakis. 2020. Quantifying fibrinogen-dependent aggregation of red blood cells in type 2 diabetes mellitus. *Biophys. J.* 119:900–912.

40. van Rooij, B. J. M., G. Závodszky, …, D. N. Ku. 2021. Haemodynamic flow conditions at the initiation of high-shear platelet aggregation: a combined *in vitro* and cellular *in silico* study. *Interface Focus.* 11:20190126.

41. Liu, Z., D. Ku, C. Aidun…, 2021. Mechanobiology of shear-induced platelet aggregation leading to occlusive arterial thrombosis: a multiscale in silico analysis. *J. Biomech.* 120:110349.

42. Ye, T., N. Phan-Thien, and C. T. Lim. 2016. Particle-based simulations of red blood cells-A review. *J. Biomech.* 49:2255–2266.

43. Li, X., H. Li, …, G. Em Karniadakis. 2017. Computational biomechanics of human red blood cells in hematological disorders. *J. Biomech. Eng.* 139:0210081–02100813.

44. Aidun, C., and J. Clausen. 2010. Lattice-Boltzmann method for complex flows. *Annu. Rev. Fluid Mech.* 42:439.

45. Li, H., H. Chang, …, G. Lykotrafitis. 2018. Modeling biomembranes and red blood cells by coarse-grained particle methods. *Appl. Math. Mech.* 39:3–20.

46. Groot, R. D., and P. B. Warren. 1997. Dissipative particle dynamics: bridging the gap between atomistic and mesoscopic simulation. *J. Chem. Phys.* 107:4423–4435.

47. Hoogerbrugge, P., and J. Koelman. 1992. Simulating microscopic hydrodynamic phenomena with dissipative particle dynamics. *EPL.* 19:155.

48. Pivkin, I. V., and G. E. Karniadakis. 2008. Accurate coarse-grained modeling of red blood cells. *Phys. Rev. Lett.* 101:118105.

49. Skalak, R., S. R. Keller, and T. W. Secomb. 1981. ASME centennial historical perspective paper: mechanics of blood flow. *J. Biomech. Eng.* 103:102–115.

50. Ku, D. N. 1997. Blood flow in arteries. *Annu. Rev. Fluid Mech.* 29:399–434.

51. Mills, J. P., L. Qie, …, S. Suresh. 2004. Nonlinear elastic and visco-elastic deformation of the human red blood cell with optical tweezers. *Mech. Chem. Biosyst.* 1:169–180.

52. Hochmuth, R. M., P. R. Worthy, and E. A. Evans. 1979. Red cell extensional recovery and the determination of membrane viscosity. *Biophys. J.* 26:101–114.

53. Fedosov, D. A. 2010. Multiscale modeling of blood flow and soft matter. Citeseer.

54. Liu, Z. L., J. R. Clausen, …, C. K. Aidun. 2020. Heterogeneous partition of cellular blood-borne nanoparticles through microvascular bifurcations. *Phys. Rev. E.* 102:013310.

55. Quinn, D. J., I. Pivkin, …, S. Suresh. 2011. Combined simulation and experimental study of large deformation of red blood cells in microfluidic systems. *Ann. Biomed. Eng.* 39:1041–1050.

56. MacDonald, I. C., D. M. Ragan, …, A. C. Groom. 1987. Kinetics of red blood cell passage through interendothelial slits into venous sinuses in rat spleen, analyzed by in vivo microscopy. *Microvasc. Res.* 33:118–134.

57. Atkinson, M., and S. Sherlock. 1954. Intrasplenic pressure as index of portal venous pressure. *Lancet.* 266:1325–1327.

58. Safeukui, I., P. A. Buffet, …, N. Mohandas. 2012. Quantitative assessment of sensing and sequestration of spherocytic erythrocytes by the human spleen. *Blood.* 120:424–430.

59. Safeukui, I., P. A. Buffet, …, N. Mohandas. 2018. Sensing of red blood cells with decreased membrane deformability by the human spleen. *Blood Adv.* 2:2581–2587.

60. Chien, S. 1970. Shear dependence of effective cell volume as a determinant of blood viscosity. *Science.* 168:977–979.

61. Fung, Y.-C. 2013. Biomechanics: Circulation. Springer Science & Business Media, New York.

62. Chien, S. 1986. Blood rheology in myocardial infarction and hypertension. *Biorheology.* 23:633–653.

63. Usami, S., S. Chien, …, J. F. Bertles. 1975. Effect of deoxygenation on blood rheology in sickle cell disease. *Microvasc. Res.* 9:324–334.

64. Peduzzi, M., M. Melli, …, F. Guerrieri. 1984. Comparative evaluation of blood viscosity in diabetic retinopathy. *Int. Ophthalmol.* 7:15–19.

65. Liu, Z., J. R. Clausen, …, C. K. Aidun. 2019. Nanoparticle diffusion in sheared cellular blood flow. *J. Fluid Mech.* 871:636–667.

66. Scherer, E. F., D. G. Cantarini, …, E. L. França. 2016. Cytokine modulation of human blood viscosity from vivax malaria patients. *Acta Trop.* 158:139–147.

67. Snabre, P., H. Bäumler, and P. Mills. 1985. Aggregation of human red blood cells after moderate heat treatment. *Biorheology.* 22:185–195.

68. Lerche, D., and H. Bäumler. 1984. Moderate heat treatment of only red blood cells (RBC) slows down the rate of RBC-RBC aggregation in plasma. *Biorheology.* 21:393–403.

69. Ujiie, H., Y. Tamano, …, T. Hori. 2001. Is the aspect ratio a reliable index for predicting the rupture of a saccular aneurysm? *Neurosurgery.* 48:495–502, discussion 502–503.

70. López, J. A., C. Kearon, and A. Y. Lee. 2004. Deep venous thrombosis. *Hematology (Am. Soc. Hematol. Educ. Program).* 2004:439–456.

71. Chien, S., S. Usami, …, M. M. Guest. 1967. Blood viscosity: influence of erythrocyte aggregation. *Science.* 157:829–831.

72. Rank, B. H., N. L. Moyer, and R. P. Hebbel. 1988. Vesiculation of sickle erythrocytes during thermal stress. *Blood.* 72:1060–1063.

73. Li, H., and G. Lykotrafitis. 2014. Erythrocyte membrane model with explicit description of the lipid bilayer and the spectrin network. *Biophys. J.* 107:642–653.

74. Li, H., and G. Lykotrafitis. 2012. Two-component coarse-grained molecular-dynamics model for the human erythrocyte membrane. *Biophys. J.* 102:75–84.

75. Razizadeh, M., M. Nikfar, …, Y. Liu. 2020. Coarse-grained modeling of pore dynamics on the red blood cell membrane under large deformations. *Biophys. J.* 119:471–482.